Comparative Modal Analysis of Grid-Following and Grid-Forming Control in a Type-3 Wind Power Plant with a Series Compensated Grid

Marcos Garcia Arregui
Centre Recherche Hydro-Québec
Hydro-Québec
Varennes, Canada
garciaarregui.marcos@hydroquebec.com

Dmitry Rimorov
Centre Recherche Hydro-Québec
Hydro-Québec
Varennes, Canada
rimorov.dmitry@hydroquebec.com

Richard Gagnon
Centre Recherche Hydro-Québec
Hydro-Québec
Varennes, Canada
gagnon.richard2@hydroquebec.com

***Abstract*—The deployment of new wind farms is accelerating across North America, particularly in Quebec. Among the available technologies, Type-3 Wind Turbines (WT) offer an attractive solution due to their ability to operate at variable speeds and their generally lower cost compared to Type-4 turbines. However, a series of Sub-Synchronous Resonance (SSR) incidents over the past decade have raised concerns among Transmission System Operators (TSOs), especially when Type-3 Wind Power Plants (WPP) are connected to series-compensated transmission lines.**

To address the challenges posed by inverter-based resources, advanced control strategies such as Grid-Forming (GFM) have emerged as promising solutions. This paper presents a small-signal model of a Type-3 WPP and evaluates both GFM and Grid-Following (GFL) control approaches in the context of a benchmark series-compensated transmission system.

***Index Terms*—wind power plant, type-3, grid forming, grid following, small-signal model**

I. Introduction

The integration of Type-3 wind turbines—characterized by Doubly-Fed Induction Generators (DFIGs)—into series-compensated transmission networks has introduced new challenges related to SSR. Several real-world events have highlighted the vulnerability of these systems under specific grid conditions. In particular we can quote incidents in Texas, Minnesota, China [1] [2] which lead to catastrophic failures.

In recent years, numerous studies have investigated the phenomenon of SSR in wind power systems. These analyses have shown that SSR can arise from the interaction between Type-3 wind turbines—specifically their induction generators and power electronic converter controls—and series-compensated transmission lines. When the instability is primarily driven by the control dynamics of the converter interacting with the series compensation, the phenomenon is referred to in the literature as Sub-Synchronous Control Interaction (SSCI) [2].

Recent literature has identified the impedance of the Rotor Side Converter (RSC) as a key contributor to SSCI instability, primarily due to its negative equivalent resistance at sub-synchronous frequencies [3] [4]. In particular, this work demonstrated that the high bandwidth of the RSC current control loop plays a critical role in triggering SSCI. While reducing the control gains could mitigate the instability, this approach significantly compromises the dynamic performance of the system and is therefore not considered a viable solution.

More recent research by [5] proposes a GFM control strategy for Type-3 wind turbines that shows promise in mitigating SSCI, even when the current control loop gains remain unchanged. This suggests that GFM control can inherently provide damping in the sub-synchronous frequency range, effectively exhibiting a positive equivalent output resistance.

The objective of this paper is to continue the work initiated by [6] and develop a small-signal model of a Type-3 GFM WPP integrated with a benchmark series-compensated transmission network. This model serves as a platform to evaluate both GFM and GFL control strategies under conditions prone to SSCI. Using modal analysis techniques, the dynamic behavior and stability characteristics of each control approach are systematically assessed, providing insights into their effectiveness in mitigating SSCI in series-compensated grid environments.

II. small-signal Model

Small-signal modeling efforts for GFL Type-3 wind turbines have already been initiated at Hydro-Québec, and a detailed description of the WPP configuration is available in [6]. The following section provides a brief overview of the existing model and outlines the key modifications introduced to accommodate the GFM control strategy. It should be noted that a linearization approach was adopted to model the wind farm. Since linearizing a nonlinear system requires all system states to be in steady-state, an *abc*-to-*dq* transformation is necessary to obtain a typical linearized state-space representation. It is crucial to clearly define all existing reference frames and their interrelationships when applying the *dq*-transformation. In particular, RSC and the Grid Side Converter (GSC) operate within an internal reference frame determined by their synchronization strategy. Each controller's state-space model is formulated in its own *dq*-reference frame. These models are subsequently transformed into a unified reference frame,

979-8-3315-8138-1

which serves as the basis for all grid-related equations in the small-signal model.

A. Benchmark series compensated grid

The proposed system contains realistic considerations for components and parameters of a wind plant interconnection. It consists of a WPP connected to an equivalent grid equivalent through a series compensated transmission line. The transmission line is represented using a standard π-model. A WPP collector system with parameters shown in Table I is used in the model.

TABLE I
BENCHMARK GRID PARAMETERS

Component	Parameters
Grid Equivalent	230 kV, $2 + j25$ Ω, 60 Hz
Series Compensation	30 Ω, 1 kA, 2.3 pu protection level
Line Data	$R_1 = 5.96$ Ω, $X_1 = 50.9$ Ω, $B_1 = 324$ μS
	Length = 100 km, continuously transposed
Main Transformer	230/34.5 kV, 115 MVA, 11.5%, X/R = 45
Collector System	$R_1 = 0.22$ Ω, $X_1 = 0.147$ Ω, $C_1 = 7.17$ μF
Turbine Transformer	34.5/0.575 kV, 115 MVA, 5.7%, X/R = 15.2

B. DFIG Based Wind Power Plant

A Type-3 wind turbine employs a DFIG connected to the turbine blades via a shaft and a gearbox. Drive train is modeled as multi-mass mode shaft. Pitch control is incorporated into the small-signal model to safeguard the turbine blades by limiting the wind turbine's power output under high wind conditions. GSC and RSC are modeled with an average model approach. The WPP includes 66 WT with the characteristics described in Table II.

It should be noted that explicit dependence on rotor speed ω_r must be introduced when linearizing DFIG equations in order to properly model the effects of the GFM control. This is contrary to GFL control strategies, where the ω_r variation is often ignored when developing a linearized model for DFIG without significant impact on the precision of such model. Modifications were necessary to successfully simulate the behavior of a DFIG under GFM control. Previous work linearized the DFIG equations around a specific operating point, ω_{r0} [6]. However, this approach is no longer valid, and ω_r must now be treated as an input to the DFIG equations in order to accurately represent its dynamics in the small-signal model.

TABLE II
DFIG PARAMETERS

Parameter	Unit	Value
P_n, V_s, V_r, f_n	VA, Vrms, Vrms, Hz	1.7×10^6, 575, 1840, 60
R_s, L_{ls}	p.u.	0.01028, 0.1543
R'_r, L'_{lr}	p.u.	0.006684, 0.1543
L_m	p.u.	3.085
H, F, p	s, p.u., –	0.56347, 0, 3

C. GFL and GFM Controls

Both control strategies utilize a *dq* decoupled cascaded control topology, sharing the same current loop and regulator tuning. The current control loop of the DFIG's RSC regulates rotor currents I_{dr} and I_{qr}. It uses PI controllers with feedforward decoupling terms to compensate for cross-coupling.The RSC current control uses a rotating reference frame aligned with stator voltages, enabling a unified control structure for both GFL and GFM modes. In this study, the current control loop settings are kept identical for both GFL and GFM control strategies.

- GFL uses a Phase Locked Loop (PLL) in order to ensure grid synchronization. If the appropriate *dq* reference angle is chosen, a decoupled control is possible allowing to control simultaneously reactive power Q injection and DFIG rotating speed ω_r. Implemented type-3 wind farm GFL in MatLab SPS model is publicly available in [7].
- GFM relies on an active power based droop control strategy to determine the synchronization angle for both the RSC and GSC. The voltage controller generates the reference magnetizing current I_{smref} based on the stator voltage magnitude feedback. I_{smref} is used then to generate I_{dqr} reference based on DFIG flux equation and impedance values. Fig. 2 summarizes the implementation in the small-signal model. The GFM control approach used in the paper is inspired by the work of [5].

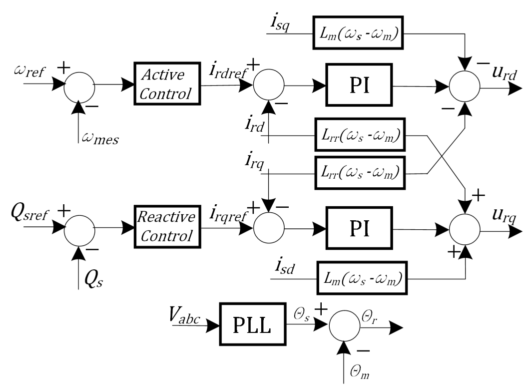

Fig. 1. GFL control current loop

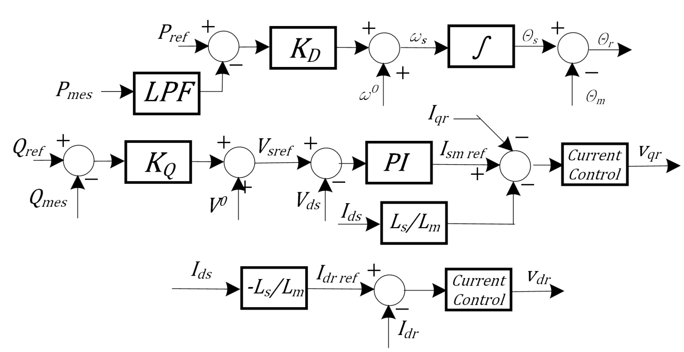

Fig. 2. GFM control

979-8-3315-8138-1

III. SMALL-SIGNAL MODEL VALIDATION

To validate the linearized system's response, a series of small perturbations were applied to its inputs and compared against the detailed nonlinear model simulated using an Electromagnetic Transient (EMT) simulation tool. It is important to note that a perfect match between the linear model and its EMT counterpart was not expected, as the latter includes all nonlinear dynamics, whereas the former represents a linearized approximation around a specific operating point.

Nevertheless, Fig. 3 confirms that the original discrete nonlinear system can be sufficiently approximated by a continuous linear model for small perturbations around a stable operating point. No tuning efforts were made to optimize control performance, as the objective of this section is to validate the dynamic behavior of the small-signal model through comparison with EMT simulation results. The GFL small-signal model was previously validated in [6], and the corresponding results are omitted here due to space constraints.

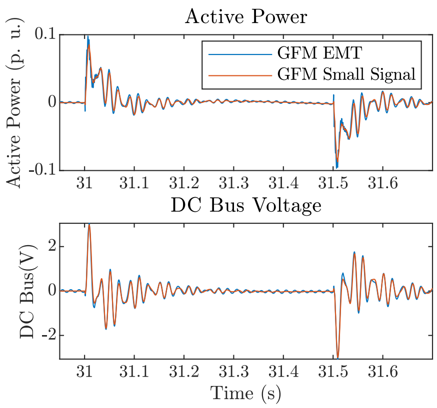

Fig. 3. GFM small-signal model validation. WPP power (top)and GSC DC bus voltage (bottom) response to $V_{q\,grid}$ steps.

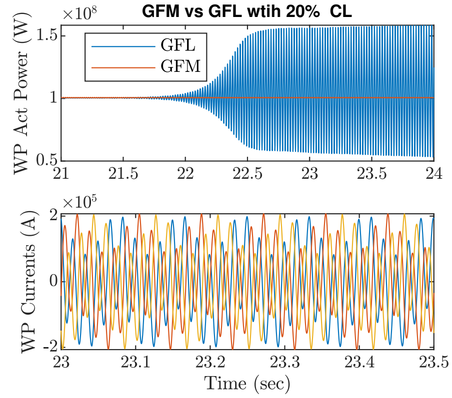

Fig. 4. Top:GFL and GFM comparison with a 20 % series compensated line. Bottom: zoom on GFL WPP current

IV. RESULTS AND DISCUSSION

A. Series compensation ratio and stability

Fig. 4 presents the EMT simulation results comparing GFM and GFL control strategies operating within the benchmark grid. As observed in the figure, the GFL control exhibits instability, while the GFM approach maintains a stable response. The lower subplot reveals an oscillatory behavior in the WPP current, with a frequency of approximately 9.8 Hz, as captured in the EMT simulation.

The modes, along with their associated frequencies and damping ratios for both control strategies, are presented in Table III and Table IV. As expected, the GFL control exhibits an eigenvalue in the right-half plane, indicating system instability. In contrast, all eigenvalues under the GFM control lie in the left-half plane, confirming a stable system response.

As it will be demonstrated in Fig. 5 and Fig. 6, the eigenvalues $\lambda_{\mathrm{GFL}1,2}$ and $\lambda_{\mathrm{GFM}1,2}$ are associated with the resonant sub-synchronous oscillation observed in Fig. 4. The small-signal model predicts an oscillation frequency of 51 Hz in the *dq* axes, which corresponds to a 9 Hz oscillation in the sequence domain [8].

TABLE III
EIGENVALUE ANALYSIS FOR GFL CONTROL

Mode(s)	Real	Imaginary	Frequency (Hz)	Damping
$\lambda_{\mathrm{GFL}1,2}$	4.1718	±320.92667	51.07707	-0.013
$\lambda_{\mathrm{GFL}6,7}$	-0.0047	±376.99034	59.99988	1e-05
$\lambda_{\mathrm{GFL}8,9}$	-0.0276	±376.98804	59.99951	7e-05
$\lambda_{\mathrm{GFL}10}$	-0.1536	0	0	1
$\lambda_{\mathrm{GFL}11}$	-0.27761	0	0	1
$\lambda_{\mathrm{GFL}12,13}$	-0.3855	±0.73973	0.11773	0.46215
$\lambda_{\mathrm{GFL}14}$	-0.96771	0	0	1
$\lambda_{\mathrm{GFL}15,16}$	-1.03606	±12.63901	2.01156	0.0817
$\lambda_{\mathrm{GFL}17,18}$	-2.31234	±6.39963	1.01853	0.33982
$\lambda_{\mathrm{GFL}19}$	-2.76312	0	0	1
$\lambda_{\mathrm{GFL}20,21}$	-7.6956	±1.88662	0.30026	0.97124
$\lambda_{\mathrm{GFL}22,23}$	-12.95566	±0.8133	0.12944	0.99804
$\lambda_{\mathrm{GFL}25,26}$	-22.3103	±426.53094	67.88451	0.05223
$\lambda_{\mathrm{GFL}27,28}$	-148.970	±78.82973	12.54614	0.88389

TABLE IV
EIGENVALUE ANALYSIS FOR GFM CONTROL

Mode(s)	Real	Imaginary	Frequency (Hz)	Damping
$\lambda_{\mathrm{GFM}1,2}$	-12.95791	±2.39728	0.38154	0.98331
$\lambda_{\mathrm{GFM}3,4}$	-0.00514	±376.99084	59.99996	10^{-5}
$\lambda_{\mathrm{GFM}4,5}$	-0.02998	±376.98974	59.99978	8×10^{-5}
$\lambda_{\mathrm{GFM}6}$	-0.27977	0	0	1
$\lambda_{\mathrm{GFM}7}$	-1.39676	0	0	1
$\lambda_{\mathrm{GFM}8,9}$	-1.41071	±12.01627	1.91245	0.1166
$\lambda_{\mathrm{GFM}10,11}$	-7.68832	±1.91714	0.30512	0.97029
$\lambda_{\mathrm{GFM}12,13}$	-10.88908	±318.67435	50.7186	0.03415
$\lambda_{\mathrm{GFM}14,15}$	-13.55759	±432.81141	68.88408	0.03131
$\lambda_{\mathrm{GFM}16,17}$	-27.13287	±31.66787	5.0401	0.65064

Table V presents the participation factors associated with the eigenvalue $\lambda_{1,2}$, which is involved in the sub-synchronous oscillation. As expected, under GFL control, the dominant contributors to mode $\lambda_{\mathrm{GFL}1,2}$ are related to the machine equations,

979-8-3315-8138-1

with a significant influence from the state variable V_{cs}, which corresponds to the voltage state across the series capacitance. These findings are consistent with the observations reported in [6] and [9].

However, under GFM control, the participation of V_{cs} is reduced by half, indicating a substantially diminished influence on the resonance mode. It is also worth noting that the machine's contribution is primarily associated with the q-axis, as the participation factors of the machine-related d-axis states, namely I_{ds} and I_{dr}, are reduced by an order of magnitude. This can be can be explained by the fact that grid-forming control is asymmetric. There is only one voltage regulator, which computes $I_{q,\mathrm{ref}}$. The value of $I_{d,\mathrm{ref}}$ is determined directly by the DFIG machine physics so that the flux remains aligned with $\phi_d = 0$. The tuning of the voltage regulator is critical for overall system stability and not only SSCI mitigation.

TABLE V
PARTICIPATION FACTORS FOR MODE $\lambda_{1,2}$

Mode	**Participation Factors**
$\lambda_{\mathrm{GFL}1,2}$	$I_{ds\_ASM} = 0.272$; $I_{qs\_ASM} = 0.22$; $I_{dr\_ASM} = 0.25$; $I_{qr\_ASM} = 0.19$; $vCs_d = 0.09$; $vCs_q = 0.09$
$\lambda_{\mathrm{GFM}1,2}$	$I_{ds\_ASM} = 0.09$; $I_{qs\_ASM} = 0.36$; $I_{dr\_ASM} = 0.04$; $I_{qr\_ASM} = 0.34$; $vCs_d = 0.04$; $vCs_q = 0.04$

Based on the previous results, a sweep of the series compensation level was performed for both control strategies, as shown in Fig. 5 and Fig. 6. It was observed that the GFL control remains stable only when the series compensation level is below 10%. The damping of $\lambda_{\mathrm{GFL}1,2}$ decreases with increasing compensation, eventually becoming negative and indicating instability. Modes $\lambda_{\mathrm{GFL}25,26}$ are as well affected by the compensation level, although with an opposite effect.

In contrast, the GFM control preserved system stability across all tested levels of series compensation within the benchmark grid. Notably, the damping of both $\lambda_{\mathrm{GFM}1,2}$ and $\lambda_{\mathrm{GFM}14,15}$ increases as the compensation level is increased.

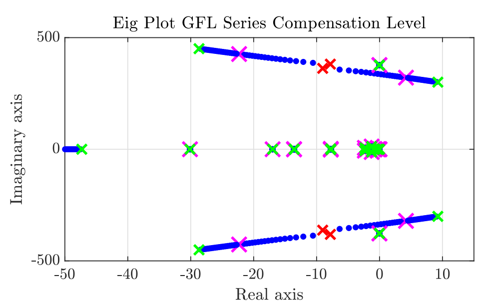

Fig. 5. GFL versus series compensation level. Red CL=0.01. Magenta CL=0.2 (benchmark grid nominal value). Green CL=0.4

B. GFL control interactions

To better understand the influence of GFL control loops on the subsynchronous resonance mode, variations in PLL bandwidth and the proportional gain of the rotor current regulator K_p are performed.

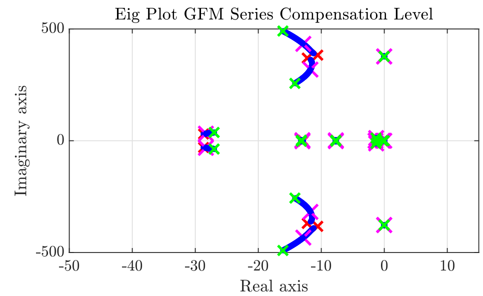

Fig. 6. GFM versus series compensation level. Red CL=0.01. Magenta CL=0.2 (benchmark grid nominal value). Green CL=0.8

As expected, reducing K_p improves the stability of the Type-3 wind farm, with full stability achieved when the gain K_p is reduced to 0.45 (Fig. 7). However, this approach cannot be considered a definitive solution, as reducing the controller gain adversely affects the dynamic performance of the wind turbine. It should also be noted that excessive reduction of the proportional gain K_p may lead the WPP toward instability, as modes $\lambda_{\mathrm{GFL}\ 27,28}$ shift into the right half of the complex plane.

In contrast, PLL bandwidth has no observable impact on modes directly associated with subsynchronous resonance, as subsynchronous modes remain unchanged despite variations in PLL bandwidth. A figure is not included due to space limitations

Finally, it is worth noting that other mitigation strategies—such as active damping—are available to address subsynchronous resonances with GFL controls, although they fall outside the scope of this paper [12].

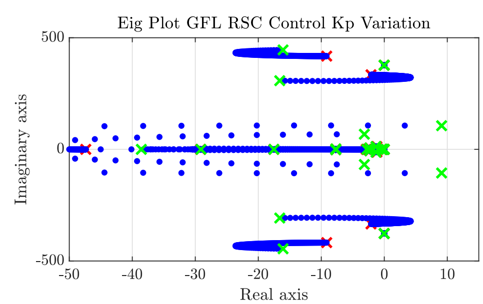

Fig. 7. GFL versus Kp RSC variation. Green Kp=0.02. Red Kp=5

C. GFM control interactions

Although the proposed GFM control strategy is stable, selected control parameters are intentionally varied toward the edge of instability to better understand their influence on system dynamics and stability margins. An eigenvalue locus is plotted while varying the parameters of the droop equation. As shown in Fig. 8, reducing the droop gain K_D has a stabilizing effect, increasing the damping of $\lambda_{\mathrm{GFM}1,2}$. On the other hand, variations in the Low-Pass Filter (LPF) time constant T_f have minimal impact on the damping of $\lambda_{\text{GFM1,2}}$ and are primarily associated with modes $\lambda_{\text{GFM8,9}}$ (Fig. 9).

Previous studies have shown that power-based synchronization in GFM control exhibits favorable damping characteristics. This can be physically explained by the fact that GFM control replicates the behavior of the swing equation of a synchronous generator. Specifically, T_f/K_D corresponds to the rotor inertia J, and $1/K_D$ represents the damping torque coefficient [10] [11]. Therefore, reducing K_D increases the damping coefficient. It should be noted, that while reducing K_D may improve small-signal stability, it can also lead to unsatisfactory transient performance, especially when the WPP experiences major grid frequency deviations. In other words, tuning K_D involves a trade-off between small-signal stability and dynamic performance. In contrast, variations in the LPF time constant have minimal impact on the sub-synchronous resonance mode $\lambda_{\text{GFM1,2}}$ damping, and its tuning should be based on the desired inertia characteristics of the GFM control.

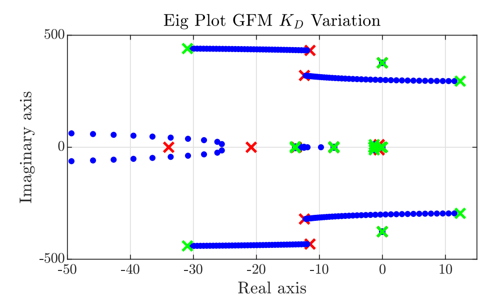

Fig. 8. GFM versus Red K_D droop variation. Red K_D = 0. Green K_D =0.4

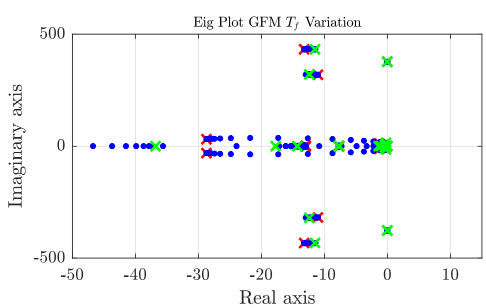

Fig. 9. GFM versus droop LPF time constant. Red T_f/K_D = 1e-5 s. Green T_f/K_D =1 s

Conclusion

A small-signal model for a Type-3 WPP was developed for both GFL and GFM control strategies. The model was tested against a series-compensated benchmark grid, and its accuracy was validated through EMT simulations. Modal analysis was then employed to gain deeper insight into the influence of control settings on a series compensated system dynamics. Based on the findings presented in this paper, Table VI summarizes the expected impact of each control loop on overall system stability. GFM exhibits superior small-signal performance compared to GFL under the proposed series-compensated benchmark grid, even when identical current control loop settings are maintained. Future work should explore whether this observation remains valid for more complex and realistic grid configurations.

TABLE VI
Expected Impact of Control Loops on Benchmark Grid

Control Loop	**Applicable**	**Expected Impact on Stability**
PLL	GFL	- No impact on subsynchronous resonance-related modes
Current Loop	GFL-GFM	- Stability improves when the proportional gain K_p is reduced
Droop Equation	GFM	- Reducing K_D enhances damping ratio and increases overall stability with series compensated grids. No major impact of T_f on series resonant modes.

Acknowledgments

The authors would like to acknowledge Aramis S. Trevisan for his valuable contributions to the GFL samll-singal modeling and code development.

References

[1] Y. Cheng et al., "Real-World Subsynchronous Oscillation Events in Power Grids With High Penetrations of Inverter-Based Resources," in *IEEE Transactions on Power Systems*, vol. 38, no. 1, pp. 316-330, Jan. 2023,

[2] Verma, N., Kumar, N., Gupta, S. et al. Review of sub-synchronous interaction in wind integrated power systems: classification, challenges, and mitigation techniques. Prot Control Mod Power Syst 8, 17 (2023)

[3] Z. Miao, "Impedance-Model-Based SSR Analysis for Type 3 Wind Generator and Series-Compensated Network," in *IEEE Transactions on Energy Conversio*n, vol. 27, no. 4, pp. 984-991, Dec. 2012.

[4] H. A. Mohammadpour and E. Santi, "Sub-synchronous resonance analysis in DFIG-based wind farms: Definitions and problem identification — Part I," *in Proc. IEEE Energy Conversion Congress and Exposition (ECCE)*, Pittsburgh, PA, USA, 2014, pp. 812-819

[5] W. Yan, S. Shah, V. Gevorgian, P. Koralewicz, R. Wallen and D. W. Gao, "On the Low Risk of SSR in Type III Wind Turbines Operating With Grid-Forming Control," in *IEEE Transactions on Sustainable Energy*, vol. 15, no. 1, pp. 443-453, Jan. 2024.

[6] Aramis S. Trevisan, Martin Fecteau, Ângelo Mendonça, Richard Gagnon, Jean Mahseredjian, "Analysis of low frequency interactions of DFIG wind turbine systems in series compensated grids", in *Electric Power Systems Research*,Volume 191. 2021.

[7] R.Gagnon, "Wind Farm - Doubly-Fed Induction Generator," in https://www.mathworks.com/help/sps/ug/wind-farm-dfig-detailed-model.html

[8] L. Harnefors, "Modeling of Three-Phase Dynamic Systems Using Complex Transfer Functions and Transfer Matrices," in *IEEE Transactions on Industrial Electronics*, vol. 54, no. 4, pp. 2239-2248, Aug. 2007

[9] A. S. Trevisan, Â. Mendonça, R. Gagnon, J. Mahseredjian and M. Fecteau, "Analytically Validated SSCI Assessment Technique for Wind Parks in Series Compensated Grids," in *IEEE Transactions on Power Systems*, vol. 36, no. 1, pp. 39-48, Jan. 2021.

[10] L. Huanget al., "Synchronization and Frequency Regulation of DFIG-Based Wind Turbine Generators With Synchronized Control," in *IEEE Trans. on Energy Conversion*, vol. 32, no. 3, pp. 1251-1262, Sept. 2017,

[11] Y. Li et al., "Impedance Circuit Model of Grid-Forming Inverter: Visualizing Control Algorithms as Circuit Elements," in *IEEE Transactions on Power Electronics*, vol. 36, no. 3, pp. 3377-3395, March 2021

[12] L. Rosado, J. Samanes, E. Gubía and J. López, "Robust Active Damping Strategy for DFIG Wind Turbines," in *IEEE Transactions on Power Electronics*, vol. 36, no. 12, pp. 14525-14538, Dec. 2021

979-8-3315-8138-1